Robust Warming Pattern of Global Subtropical Oceans and Its Mechanism

GUIHUA WANG

State Key Laboratory of Satellite Ocean Environment Dynamics, Second Institution of Oceanography, State Oceanic Administration, Hangzhou, China

SHANG-PING XIE

Scripps Institution of Oceanography, University of California, San Diego, La Jolla, California, and Physical Oceanography Laboratory, and Qingdao Collaborative Innovation Center of Marine Science and Technology, Ocean University of China, Qingdao, China

RUI XIN HUANG

Woods Hole Oceanographic Institution, Woods Hole, Massachusetts

CHANGLIN CHEN

State Key Laboratory of Satellite Ocean Environment Dynamics, Second Institution of Oceanography, State Oceanic Administration, Hangzhou, China

(Manuscript received 26 November 2014, in final form 11 August 2015)

ABSTRACT

The subsurface ocean response to anthropogenic climate forcing remains poorly characterized. From the Coupled Model Intercomparison Project (CMIP), a robust response of the lower thermocline is identified, where the warming is considerably weaker in the subtropics than in the tropics and high latitudes. The lower thermocline change is inversely proportional to the thermocline depth in the present climatology. Ocean general circulation model (OGCM) experiments show that sea surface warming is the dominant forcing for the subtropical gyre change in contrast to natural variability for which wind dominates, and the ocean response is insensitive to the spatial pattern of surface warming. An analysis based on a ventilated thermocline model shows that the pattern of the lower thermocline change can be interpreted in terms of the dynamic response to the strengthened stratification and downward heat mixing. Consequently, the subtropical gyres become intensified at the surface but weakened in the lower thermcline, consistent with results from CMIP experiments.

1. Introduction

Global surface temperature is projected to rise a few degrees by 2100. Oceans absorb 93% of heat imbalance at the top of the atmosphere (Church et al. 2011; Levitus et al. 2012; Balmaseda et al. 2013), and this ocean heat storage slows down the rate of surface warming and causes sea level to rise. Oceans are in motion, and the heat transport by changing currents affects atmospheric circulation and regional climate (Zhang and Delworth 2005; Timmermann et al. 2007).

The anticyclonic subtropical gyres are driven by wind stress curls between the westerlies in the midlatitudes and trade winds in the tropics. They hold the largest volume of warm water (say, temperature $> 10°C$) in the world's oceans. In light of the importance of the subtropical gyres for climate (Kobashi and Kubokawa 2012; Qiu and Chen 2013; Crandall et al. 2014), marine ecosystems (Karl et al. 1995; Corno et al. 2007), and biogeochemistry (Letelier et al. 2000), it is crucial to know how the oceanic gyres will change in the face of climate warming.

Recent studies have considered the effect of wind stress changes on the subtropical gyres (Cowan et al.

Corresponding author address: Guihua Wang, Second Institute of Oceanography, State Oceanic Administration, 36 North Bao-Chu Road, Hangzhou 310012, China.
E-mail: wghocean@yahoo.com

DOI: 10.1175/JCLI-D-14-00809.1

2013; Zhang et al. 2014). The wind stress changes also play significant roles in spinning up the poleward edge of the subtropical gyre (Kuroshio recirculation; Sakamoto et al. 2005) and enhancing the equatorial heat content and sea level rise (Yin et al. 2010; Timmermann et al. 2010). Stratification is another factor regulating the inertial recirculation. The surface recirculation can be strengthened with increased stratification (Sun et al. 2013). The change in the surface heat flux can reduce the amount of the central mode water (Xu et al. 2012) and can further enhance the heat content in the recirculation gyre by decreasing the mode water thickness (Luo et al. 2009).

Generally, the robust changes in the subtropical gyres common to all basins remain to be fully characterized and the underlying mechanisms are poorly understood. Using a hierarchy of models, we show that there are robust patterns of the subtropical gyre response to global warming, and they are distinct from natural variability in both structure and mechanism. The paper is structured as follows. In section 2, model output, model formulation, and parameterization are described. In section 3, we examine the ocean response to climate change with output from phase 5 of the Coupled Model Intercomparison Project (CMIP5) and investigate the effects of sea surface temperature (SST), sea surface salinity (SSS), and wind changes on the ocean response with an ocean general circulation model (OGCM). Finally we use a ventilated thermocline model to interpret the ocean response and identify causes. Section 4 is a summary with discussion.

2. Methodology

a. CMIP5 output

Historical and representative concentration pathway 4.5 (RCP4.5) runs from 36 available models from CMIP5 (Taylor et al. 2012; http://pcmdi9.llnl.gov/esgf-web-fe/; also see Table 1) are used to represent the present-day and warmer climates, respectively. The differences between RCP4.5 (2076–2100) and historical experiments (1976–2000) are used to explore the ocean response to climate change. The output is provided on various grids and regridded onto a common $1^\circ \times 1^\circ$ grid and 33 vertical levels for analysis.

b. Ocean model

The OGCM is Océan Parallélisé in Nucleus for European Modelling of the Ocean (NEMO-OPA; Madec 2008). NEMO-OPA is a dynamic–thermodynamic model specifically designed for climate studies. The model is configured on a tripolar horizontal mesh of approximately 1° resolution with a tropical refinement to 1/3° (ORCA1). The model has 46 levels in the vertical direction, with the layer thicknesses ranging from 6 m at the surface to 250 m at the ocean bottom. To give better topographic representation, the partial step scheme is applied to the bottom grid cell; thus, the thickness in the bottom grid cell can vary with location. All spatial grid schemes were developed by the DRAKKAR Consortium (Barnier et al. 2007).

The vertical viscosity and diffusion coefficient are parameterized using a one-equation turbulent kinetic energy (TKE) scheme (Blanke and Delecluse 1993). Lateral diffusion by eddies is parameterized (Gent and Mcwilliams 1990). The eddy-induced velocity coefficient is calculated by the model based on the baroclinicity of the ocean at each time step. A harmonic viscosity scheme is used with a spatially varying coefficient ranging from $1 \times 10^3\,\mathrm{m^2\,s^{-1}}$ in the tropics to $1 \times 10^4\,\mathrm{m^2\,s^{-1}}$ poleward of 20°N and 20°S.

To reach the quasi-equilibrium state, the model is first integrated for 100 years, forced by the climatological monthly Coordinated Ocean–Ice Reference Experiments, version 2 (CORE2), data (Large and Yeager 2009). Afterward, the 36-model ensemble mean wind, SST, and SSS fields from CMIP5 are used to drive the ocean model for 125 years from 1976 to 2100 in six experiments. The surface forcings are separated into two parts: one is the monthly climatology from CMIP5 historical experiments and the other is the change from 1976 to 2100. The average of the last 25 years (2076–2100) of each experiment is used in the analysis presented here. The differences in forcing (Table 2) among experiments are used to present the response by full forcing, wind change only, SST change only, SSS change only, and globally uniform SST change only. SST and SSS are strongly restored toward the CMIP5 data by using restoring conditions for both surface heat flux and freshwater flux. The restoring coefficient is $120\,\mathrm{W\,m^{-2}\,K^{-1}}$ for SST and $166\,\mathrm{mm\,day^{-1}}$ for SSS.

Surface heat flux is often parameterized as Newtonian damping, but the restoring we employed in our experiments (20 days) is stronger. As a test, we doubled the restoring time; the results obtained are qualitatively similar to the results obtained under strong relaxation. Indeed, our OGCM simulation (see Fig. 6a) largely reproduced coupled mode results (see Fig. 2a).

c. Ventilated thermocline model

1) Model formulation and parameters

The model follows the formulation of Luyten et al. (1983) and Huang (2010). It includes two ventilated layers (with potential density ρ_1 and ρ_2) and a stagnant bottom layer (with potential density ρ_3). The second

TABLE 1. 36 CMIP5 models used in this study (Flato et al. 2013). (Expansions of model name acronyms are available at http://www.ametsoc.org/PubsAcronymList.)

Model	OGCM resolution (lon grid points× lat grid points × levels)	Institution, country
ACCESS1.0	360 × 300 × 50	Commonwealth Scientific and Industrial Research Organisation (CSIRO) and Bureau of Meteorology, Australia.
ACCESS1.3		
BCC_CSM1.1	360 × 232 × 40	Beijing Climate Center, China Meteorological Administration, China.
BCC_CSM1.1(m)		
BNU-ESM	360 × 200 × 50	College of Global Change and Earth System Science, Beijing Normal University, China.
CanESM2	256 × 192 × 40	Canadian Centre for Climate Modelling and Analysis, Canada.
CCSM4	320 × 384 × 60	National Center for Atmospheric Research (NCAR), United States
CESM1(BGC)[a]		
CESM1(CAM5)		
CMCC-CM	182 × 149 × 31	Centro Euro-Mediterraneo per i Cambiamenti Climatici, Italy
CMCC-CMS		
CNRM-CM5	362 × 292 × 42	Centre National de Recherches Météorologiques, France
CSIRO Mk3.6.0	192 × 189 × 31	CSIRO and Queensland Climate Change Centre of Excellence, Australia
EC-EARTH	362 × 292 × 42	European Earth System Model consortium, Europe
FGOALS-g2	360 × 196 × 30	Institute of Atmospheric Physics, Chinese Academy of Sciences, China
FGOALS-s2		
FIO-ESM	320 × 384 × 40	First Institute of Oceanography, State Oceanic Administration, China
GFDL CM3	360 × 200 × 50	NOAA/Geophysical Fluid Dynamics Laboratory, United States
GFDL-ESM2G	360 × 210 × 50	
GFDL-ESM2M	360 × 200 × 50	
GISS-E2-H-CC	144 × 90 × 33	NASA Goddard Institute for Space Studies, United States
GISS-E2-R	288 × 180 × 32	
GISS-E2-R-CC		
HadGEM2-CC	360 × 216 × 40	Met Office Hadley Centre, United Kingdom
HadGEM2-ES		
IPSL-CM5A-LR	182 × 149 × 31	L'Institut Pierre-Simon Laplace, France.
IPSL-CM5A-MR		
IPSL-CM5B-LR		
MIROC5	256 × 224 × 50	Japan Agency for Marine-Earth Science and Technology, Atmosphere and Ocean Research Institute, and National Institute for Environmental Studies, Japan
MIROC-ESM-CHEM	256 × 192 × 44	
MIROC-ESM		
MPI-ESM-LR	256 × 220 × 40	Max Planck Institute for Meteorology, Germany
MPI-ESM-MR	802 × 404 × 40	
MRI-CGCM3	360 × 368 × 51	Meteorological Research Institute, Japan
NorESM1-M	320 × 384 × 70	Norwegian Climate Centre, Norway
NorESM1-ME		

[a] BGC is biogeochemistry.

layer outcrops at middle latitudes (Fig. 1). In the ocean interior, the time-dependent frictional and inertial terms are negligible. Assuming equilibrium holds in the ventilated thermocline model, the zonal integration of the Sverdrup relation yields the total layer thickness,

$$h^2 = \frac{1}{\Delta}\left[h_e^2 - \frac{2f^2}{g'\beta\rho_0}W_e(x_e - x)\right] \quad \text{and}$$

$$\Delta = 1 + (\gamma + 1)\left(1 - \frac{f}{f_1}\right)^2, \tag{1}$$

where h is the total thickness of the moving layers, h_e is the upper-layer thickness along the eastern boundary, f is the Coriolis parameter and f_1 is its value at the outcrop line $y = y_1$, $\beta = df/dy$, $g' = g(\rho_3 - \rho_2)/\rho_0$ is the reduced gravity ($\rho_0 = 1028.0\,\mathrm{kg\,m^{-3}}$), W_e is the wind stress–induced Ekman pumping, and $\gamma = (\rho_3 - \rho_1)/(\rho_3 - \rho_2)$.

The thickness of the upper layer h_1 and lower layer h_2 obeys

$$h_1 = \left(1 - \frac{f}{f_1}\right)h \quad \text{and} \tag{2}$$

$$h_2 = \frac{f}{f_1}h, \tag{3}$$

respectively. The momentum equations of the first and second layers are

TABLE 2. Forcing set for NEMO-OPA experiments. The overline denotes the monthly climatology from CMIP5 historical experiments (1976–2000), and the prime denotes the change from 1976 to 2100.

Expt name	Forcings			Motivation
	Wind (W)	SST (T)	SSS (S)	
CTR	$\overline{W}$	$\overline{T}$	$\overline{S}$	Control run
FULL	$\overline{W}+W'$	$\overline{T}+T'$	$\overline{S}+S'$	Response to global warming
EXP(WIND)	$\overline{W}+W'$	$\overline{T}$	$\overline{S}$	Role of wind stress change
EXP(SST)	$\overline{W}$	$\overline{T}+T'$	$\overline{S}$	Role of SST change
EXP(SSS)	$\overline{W}$	$\overline{T}$	$\overline{S}+S'$	Role of SSS change
EXP(uSST)	$\overline{W}$	$\overline{T}+\text{mean}(T')$	$\overline{S}$	Role of spatially uniform SST change (the change value is global mean)

$$fv_1 = g'\frac{\partial}{\partial x}(\gamma h_1 + h_2), \quad fu_1 = -g'\frac{\partial}{\partial y}(\gamma h_1 + h_2) \tag{4}$$

and

$$fv_2 = g'\frac{\partial}{\partial x}(h_1 + h_2), \quad fu_2 = -g'\frac{\partial}{\partial y}(h_1 + h_2), \tag{5}$$

respectively.

Unless stated otherwise, all parameters in the ventilated thermocline model are extracted from historical and RCP4.5 experiments of CMIP5. These parameters (Table 3) are used to drive the simple model in five experiments: 1) all parameters are from historical experiments (control run), 2) all parameters are from RCP4.5 experiments, 3) stratification change only, 4) h_e change only, and 5) f_1 change only.

2) PHYSICS OF CLIMATE CHANGE IN VENTILATED THERMOCLINE MODEL

Climate change in this simple model can be examined by taking the difference of Eq. (1),

$$\delta h = \underbrace{\frac{h_e}{h}\delta h_e}_{\text{term I}} \underbrace{-\frac{h}{2}\frac{\delta g'}{g'}\left(1-\frac{h_e^2}{\Delta h^2}\right)}_{\text{term II}} \underbrace{-\frac{f^2}{\Delta h g'\beta\rho_0}(x_e - x)\delta W_e}_{\text{term III}} + \underbrace{\frac{(\gamma-1)\left(1-\frac{f}{f_1}\right)\frac{f}{f_1^2}}{\Delta}h\delta f_1}_{\text{term IV}}, \tag{6}$$

where δ denotes the difference of RCP4.5 minus historical experiments. We assume γ and other parameters are fixed and focus on the corresponding physics associated with δh_e, $\delta g'$, δW_e, and δf_1.

- Term I: Vertical mixing effect increases h_e; $\delta h_e = 65$ m (increases from 485 to 550 m). The induced thermocline deepening is inversely proportional to the mean thermocline depth.
- Term II: Surface warming enhances the stratification; $\delta\rho_1 = -0.5\,\text{kg m}^{-3}$ and $\delta\rho_2 = -0.25\,\text{kg m}^{-3}$, so that $\delta g' = 0.25\,\text{cm s}^{-2} > 0$, and $\gamma = 2$ is fixed in this study [note that results are not sensitive to slight changes in γ; the general case of $\delta\gamma \neq 0$ can be handled easily since Eq. (1) is directly used in experiments]. The thermocline becomes shallower, and the shoaling is linearly proportional to the mean thermocline depth.
- Term III: Change in Ekman pumping induced by wind stress variability. The contribution of this term is small, a result supported by OGCM results as reported below.
- Term IV: Poleward migration of the outcrop line. Surface warming induces a 4° poleward shift of the outcrop line ($\delta f_1 > 0$), and the resulting thermocline shoaling is linearly proportional to the mean thermocline depth.

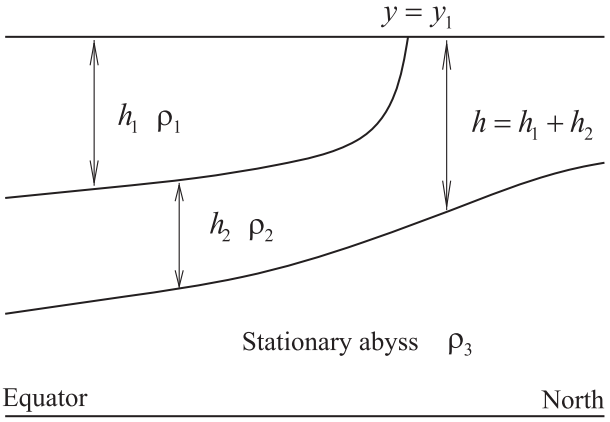

FIG. 1. Sketch of a 2.5-layer model of the ventilated thermocline in a subtropical basin.

TABLE 3. Ventilated thermocline model parameters.

Test	Parameters
Control	Outcrop line set to 38°N. Layer densities are $\rho_1 = 1023.5\,\mathrm{kg\,m^{-3}}$, $\rho_2 = 1025.5\,\mathrm{kg\,m^{-3}}$, and $\rho_3 = 1027.5\,\mathrm{kg\,m^{-3}}$. Wind from historical experiment from CMIP5. Upper-layer thickness along the eastern boundary (h_e) from historical experiment from CMIP5.
h_e	Same as control, but h_e changed to RCP4.5 experiments.
Stratification	Same as control, but $\rho_1 = 1023\,\mathrm{kg\,m^{-3}}$ and $\rho_2 = 1025.3\,\mathrm{kg\,m^{-3}}$.
Outcrop line	Same as control, but outcrop line is set to 42°N.
Full	Change h_e, stratification and outcrop line as in the above three experiments.

3. Results

a. Subtropical gyre change from CMIP5 models

We analyze global warming projections by 36 models from CMIP5. The change of the 10°C isotherm depth (Fig. 2) over the twenty-first century demonstrates the warming pattern of the lower thermocline. The mean 10°C isotherm depth is 400–1000 m in the subtropics. As the upper ocean warms globally, the 10°C isotherm depth deepens in a coherent pattern: the isotherm deepening is small in the subtropics where it is deep in climatology, while the deepening is large in the low and high latitudes where it is shallow in climatology. Within the subtropical gyres, the deepening of the 10°C isotherm depth weakens westward as the climatology deepens. Generally, the deepening of the 10°C isotherm depth is inversely proportional to its climatological depth (Figs. 3a,b).

Because of the warm salty overflow waters in the Mediterranean and Red Seas, the mean depth of the 10°C isotherm is deep in the northeastern Atlantic Ocean and western Indian Ocean, respectively. Accordingly, their changes are small compared to other regions. To make all basins more directly comparable, we plotted the $\sigma_0 = 26.8\,\mathrm{kg\,m^{-3}}$ isopycnal depth and its change (Fig. 2b). The climatological mean isopycnal depth in both the northeastern Atlantic Ocean and the western Indian Ocean is relatively shallow, and its pattern looks more like the pattern in other gyres. The pattern in these two basins demonstrates that the change of the isopycnal depth is inversely proportional to the isopycnal depth climatology like the other oceans. The isopycnal depth change is linearly linked to its climatological mean in all subtropical oceans (Fig. 3c).

Globally averaged, the 10°C isotherm in the subtropics deepens by 44 m over the twenty-first century,

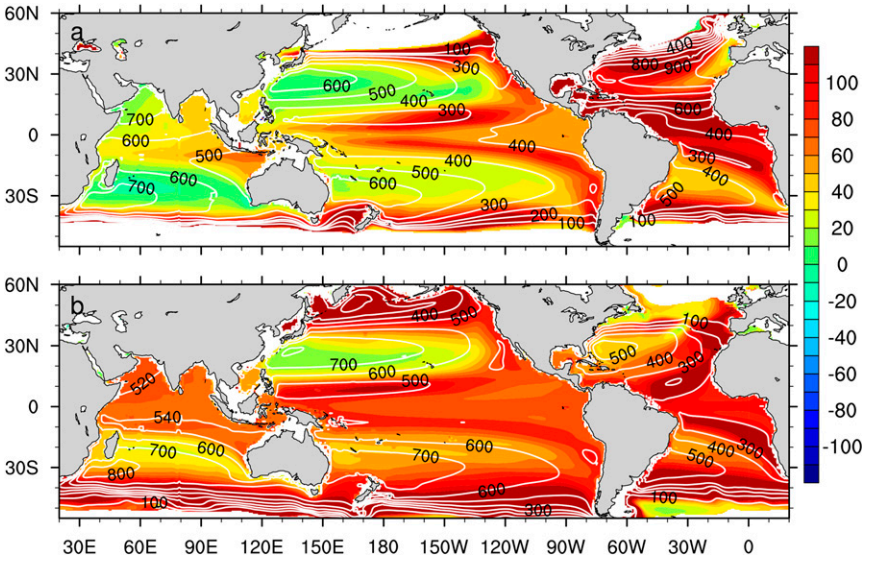

FIG. 2. Climatology (white contours; m) and change (color; m) of (a) the 10°C isotherm depth and (b) the $\sigma_0 = 26.8\,\mathrm{kg\,m^{-3}}$ isopycnal depth from 1976–2000 to 2076–2100 from 36 CMIP5 models. Positive change in color maps means deepening of isotherm and isopycnal depth. The change is defined as the differences between the RCP4.5 and historical experiments. The mean is the climatology for historical experiments.

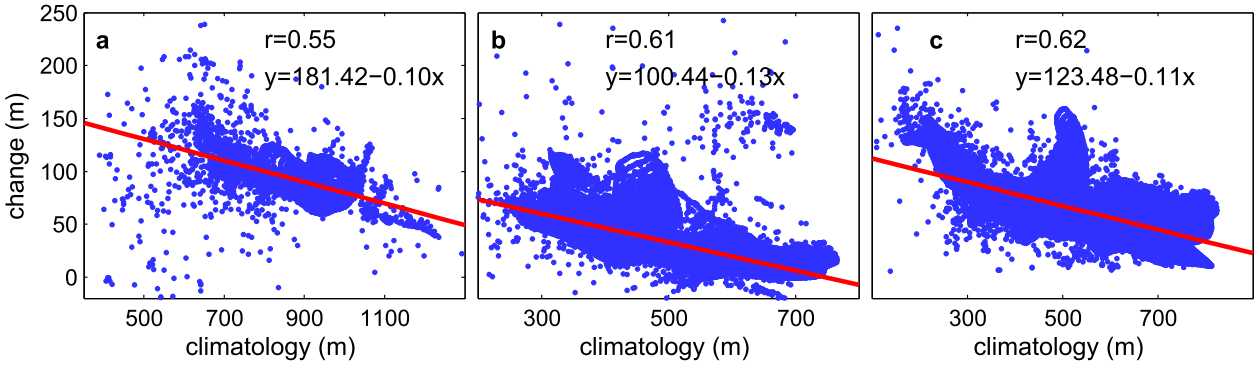

FIG. 3. Scatterplot between the mean and change of (a) the 10°C isotherm depth (m) for the subtropical North Atlantic Ocean. (b) As in (a), but for other subtropical oceans. (c) The $\sigma_0 = 26.8\,\mathrm{kg\,m^{-3}}$ isopycnal depth for all subtropical basins. In each panel, r is the spatial correlation and the red line is the linear fit. The change is defined as the differences between the RCP4.5 and historical experiments. The climatological mean is for historical experiments.

which corresponds to two-thirds of the change in equatorial oceans and one-half of that in subpolar regions (Table 4). Almost all CMIP5 models show the common warming pattern, with smaller changes of the 10°C isotherm depth in the subtropics than in low and high latitudes (Fig. 4). On depth coordinates, the zonally averaged temperature change shows a tongue of reduced warming from 300 to 1500 m in the subtropics for each basin (Fig. 5, top).The zonally averaged potential density change exhibits a similar tongue where the potential density is increased from 300 to 1500 m in the subtropics (Fig. 5, bottom).

b. *Effects of wind, SST, and SSS in OGCMs*

To investigate the cause of the subtropical change discussed above, we used the NEMO-OPA OGCM. The spatial pattern of the change of $\sigma_0 = 26.8\,\mathrm{kg\,m^{-3}}$ isopycnal depth (Fig. 6a) due to changes in wind, SST, and SSS (full-forcing experiment later) is quite similar to the CMIP5 36-model ensemble mean (Fig. 2). They both show that the $\sigma_0 = 26.8\,\mathrm{kg\,m^{-3}}$ isopycnal depth in the subtropics increases much less than at low and high latitudes in all basins. Generally, the OGCM captures the main features of the lower thermocline response to climate change. The OGCM experiment forced by SST change only (Fig. 6b) almost reproduces the results of the full-forcing experiment (Fig. 6a). Their spatial correlation is 0.97, with almost the same magnitude. In all basins, except the North Atlantic Ocean, the pattern of isopycnal depth change induced by SSS change is generally similar to that resulting from SST change, with a much weaker magnitude. Their patterns are similar because of the out-of-phase relationship between SST and SSS in climate change (Terray et al. 2012; Durack et al. 2012). In the North Atlantic, both SST and SSS are increased south of 40°N, while SST is increased slightly and SSS is decreased north of 40°N; thus, the $\sigma_0 = 26.8\,\mathrm{kg\,m^{-3}}$ isopycnal depth change induced by SSS change is generally opposite of the change induced by SST, with a much weaker magnitude.

Compared to the SST and SSS experiments, the pattern of the $\sigma_0 = 26.8\,\mathrm{kg\,m^{-3}}$ isopycnal depth change induced by wind change is totally different from the full-forcing experiment (spatial correlation of 0.09), and the magnitude is very small (Fig. 6c). The four experiments highlight the dominant effect of buoyance forcing (in particular, SST) in the lower thermocline response to climate warming, in sharp contrast to the natural variability primarily induced by wind forcing (Qiu and Chen 2005; Taguchi et al. 2007). This differs from the tropical surface circulation response in which the wind effect is important (Timmermann et al. 2010).

We carried out another experiment with a uniform SST warming to test the effect of the spatial pattern of SST change. The spatial pattern of the $\sigma_0 = 26.8\,\mathrm{kg\,m^{-3}}$ isopycnal depth change bears a striking resemblance to that in the full-forcing experiment (Fig. 6d; spatial correlation of 0.84), with a slightly larger magnitude. This

TABLE 4. Change of the 10°C isotherm depth (m) from the CMIP5 model ensemble.

	North Pacific	South Pacific	North Atlantic	South Atlantic	South Indian	Global
Equatorial latitudes (0°–15°N/S)	56	51	152	51	41	64
Subtropical latitudes (15°–35°N/S)	34	32	93	31	15	44
Subpolar latitudes (35°–50°N/S)	69	86	153	86	77	92

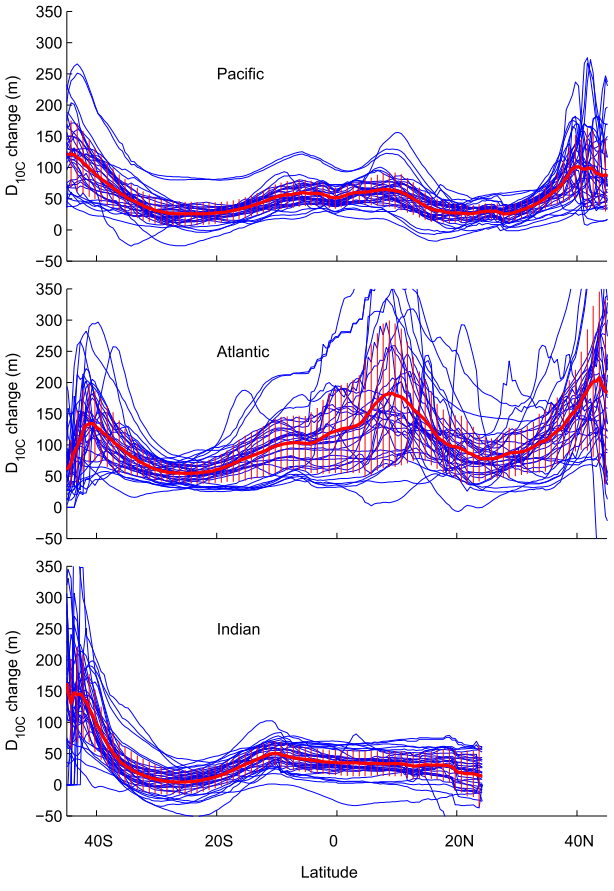

FIG. 4. Change in zonally averaged isotherm depth of 10°C from 36 CMIP5 models (blue line). Thick red lines are the ensemble mean, and thin vertical red lines are the standard deviations. The change is defined as the differences between the RCP4.5 and historical experiments.

result suggests that the $\sigma_0 = 26.8\,\mathrm{kg\,m^{-3}}$ isopycnal depth change is mainly determined by the amplitude of SST change but is insensitive to the spatial distribution of the SST forcing. The mean temperature rise since the 1950s is of high confidence, although the spatial pattern is still under debate (Deser et al. 2010; Tokinaga et al. 2012). The insensitivity of these results to the SST warming pattern suggests that the response pattern of the lower thermocline in the subtropics is robust.

In these OGCM experiments, the response of the lower thermocline is produced by an ensemble mean forcing. Can the response pattern be simulated from the mean of experiments with the forcing of each individual CMIP5 model? Considering expensive computations, we repeat these experiments with just the forcing of the GFDL-ESM2M coupled model only. The response is almost the same (figures not shown), suggesting that the response pattern of the lower thermocline is robust. In addition, all output of 36 CMIP5 models demonstrates the same response pattern, suggesting that the response pattern results from fairly simple dynamical–thermodynamic processes.

c. *Mechanisms for change inferred from a ventilated thermocline model*

We use a simple ventilated thermocline model to isolate essential dynamics and identify important features of ocean adjustments to global warming. The 2.5-layer model is widely used and capable of simulating the major structure of the main thermocline. Since the lower thermocline response to climate change is qualitatively the same for all basins, we show results for the North Pacific only. As in the OGCM, the effect of wind change is unimportant. Thus, our discussion here is focused on the effect of changes in density stratification, thermocline depth at the eastern boundary, and the position of the outcrop line due to warming. With these three factors included, the simple model reproduces the $\sigma_0 = 26.8\,\mathrm{kg\,m^{-3}}$ isopycnal depth change in CMIP5 well (spatial correlation of 0.66), characterized by a cyclonic anomaly with the reduced isopycnal depth change in the western subtropical gyre and large isopycnal depth change around the edge of the subtropical gyre (Figs. 7a and 7b). This result indicates that the simple ventilation model retains the dynamics essential for the description of climate change in the lower thermocline. Zonal variations of the isopycnal depth change in the eastern Pacific are much more gradual in the 2.5-layer model than in CMIP5 and NEMO-OPA. This discrepancy may be due to limitations of the simple model. For example, the simple model cannot produce the eastern boundary layer because all viscous forces are excluded (Vallis 2006). In addition, this simple model does not include the mixed layer; hence, the dynamic effect of spatial variations in the mixed layer depth is excluded from the model.

The ocean surface warming affects the thermocline as follows. First, the vertical diffusion of surface warming lowers isopycnals downward. This vertical mixing effect is represented in the 2.5-layer model as an increase in isopycnal depth along the eastern boundary. Averaged along the eastern boundary in CMIP5, the $\sigma_0 = 26.8\,\mathrm{kg\,m^{-3}}$ isopycnal depth increases from 485 m (historical run) to 550 m (RCP4.5 run). The deepening of the $\sigma_0 = 26.8\,\mathrm{kg\,m^{-3}}$ isopycnal depth along the eastern boundary is caused by complicated adjustments of the wind-driven and thermohaline circulation. The wind, SST, and SSS can also contribute to the increase of the $\sigma_0 = 26.8\,\mathrm{kg\,m^{-3}}$ isopycnal depth via other oceanic processes, such as Southern Ocean Ekman- and eddy-induced transport, North Atlantic Deep Water formation (Marshall and Zanna 2014). Mixing is important

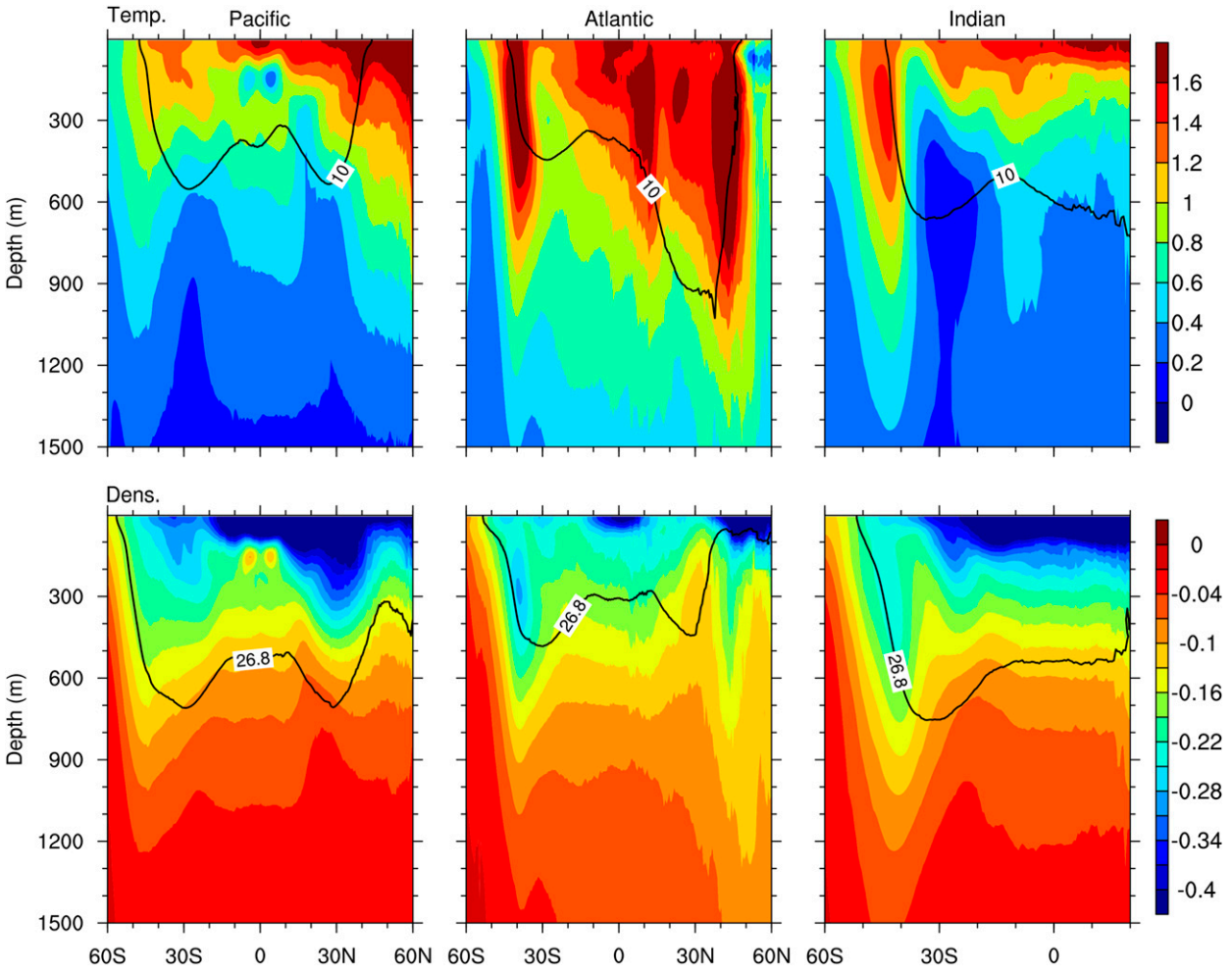

FIG. 5. (top) Zonally averaged temperature change (°C) and (bottom) density change (kg m^{-3}) for individual basins from the 36-model CMIP5 ensemble. Black lines in (top) are the zonally averaged isotherm depth of 10°C and in (bottom) the isopycnal depth of σ_0 = 26.8 kg m^{-3} for historical experiments. The change is defined as the differences between the RCP4.5 and historical experiments.

along boundaries (Gnadadesikan 1999), and the deepening of the $\sigma_0 = 26.8\,\mathrm{kg\,m^{-3}}$ isopycnal depth can reach 90 m on average through mixing as the surface is warming from 18.4°C (from CMIP5 historical simulations) to 20.3°C (from RCP 4.5 simulations) at the eastern boundary. Here we use average vertical eddy diffusivity ($1.3 \times 10^{-4}\,\mathrm{m^2\,s^{-1}}$) and vertical velocity ($1.2\,\mathrm{cm\,day^{-1}}$) taken from Munk (1966), although the magnitude of the eddy diffusivity is still under debate (Church et al. 1991; Marshall and Zanna 2014). Our simple model does not consider explicitly processes such as eddy-induced transport and North Atlantic Deep Water formation. Instead we simply take them as part of the diapycnal mixing (Gnanadesikan 1999). The increase of the $\sigma_0 = 26.8\,\mathrm{kg\,m^{-3}}$ isopycnal depth along the eastern boundary causes the thermocline to deepen in the interior ocean (Fig. 7c). Since this effect is inversely proportional to the mean thermocline depth [term I in Eq. (6); see section 2c], the $\sigma_0 = 26.8\,\mathrm{kg\,m^{-3}}$ isopycnal depth deepening is strongly reduced in the western subtropical gyre.

Second, surface warming strengthens the density stratification. Enhanced stratification shoals the thermocline throughout the subtropical gyre to satisfy Sverdrup dynamics (Fig. 7d). The thermocline shoaling is linearly proportional to the mean thermocline depth [term II in Eq. (6); see section 2c]. Both the enhanced stratification and vertical mixing reduce the deepening of the lower thermocline in the subtropical gyre. Characteristic of CMIP5 and the OGCM results, the westward-intensified reduction in the $\sigma_0 = 26.8\,\mathrm{kg\,m^{-3}}$ isopycnal depth change is strongly linked to the climatological-mean isopycnal depth distribution, as is illustrated by the simple model analysis here.

Third, because of the surface density decrease, the outcrop line is displaced poleward in warmer climate.

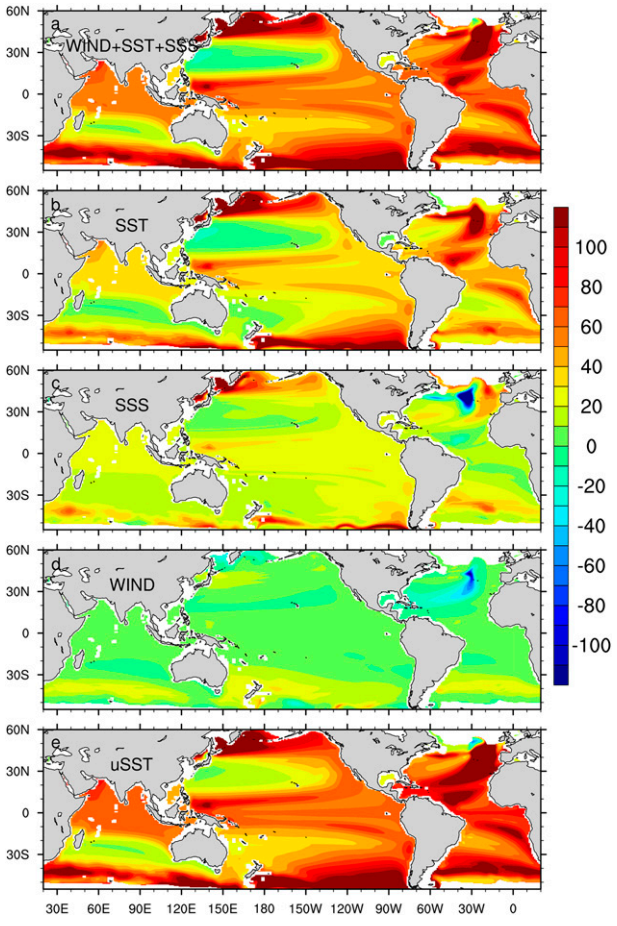

FIG. 6. Change of $\sigma_0 = 26.8\,\mathrm{kg\,m^{-3}}$ isopycnal depth (m) in OGCM experiments considering different forcings by (a) wind, SST, and SSS change; (b) SST change only; (c) SSS change only; (d) wind change only; and (e) globally uniform SST change. The change is defined as the differences between the RCP4.5 and historical experiments.

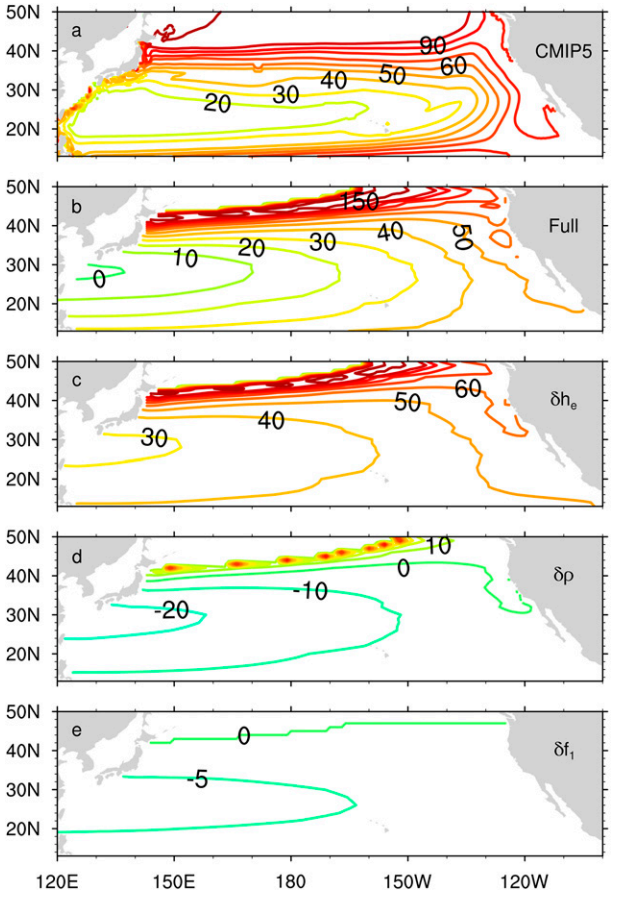

FIG. 7. (a) Change of $\sigma_0 = 26.8\,\mathrm{kg\,m^{-3}}$ isopycnal depth (m) taken from CMIP5. Lower-layer depth change (m) from a ventilated thermocline model of the North Pacific forced by (b) the full forcing, (c) layer deepening along the east boundary only, (d) density change only, and (e) northward shift of the outcrop line only. The change is defined as the differences between the RCP4.5 and historical experiments.

Although this effect is minor on the lower thermocline depth (Fig. 7e), it is important for the baroclinic flow structure between the upper and lower layers [Eqs. (2) and (3), respectively; see section 2c]. The ventilation model predicts that the poleward shift of the outcrop line causes an anomalous anticyclonic and cyclonic circulation in the upper and lower layers, respectively (Figs. 8a and 8b). The circulation change integrated over the upper 300 m and over the intermediate layer from 300 to 1000 m in CMIP5 confirms this prediction (Figs. 8c and 8d). In CMIP5, the center of the lower-layer anomalous cyclonic circulation is displaced slightly south of that of the upper-layer anomalous anticyclonic circulation, a feature the simple model captures. The change patterns of upper- and lower-layer circulation can also be seen in heat storage (color shading in Figs. 8c and 8d). The subtropical heat storage is much less than the low and high latitudes in the lower layer, while it is larger than the low and high latitudes in the upper layer. The agreement between CMIP5 and the simple model supports our hypothesis that the outcrop line shift is important in the volume transport partitioning of the subtropical gyre between the upper and lower thermocline.

4. Summary and discussion

In conclusion, our study reveals a robust pattern of the subtropical gyre response to global warming, a pattern common to all CMIP5 models. Under surface warming, vertical mixing causes isopycnals to deepen: the isopycnal deepening is not uniform but is reduced in the subtropical gyres, especially in the western basin. Our OGCM experiments show that the surface warming is the dominant cause of this pattern of subsurface change, with little contribution from wind change. Our results

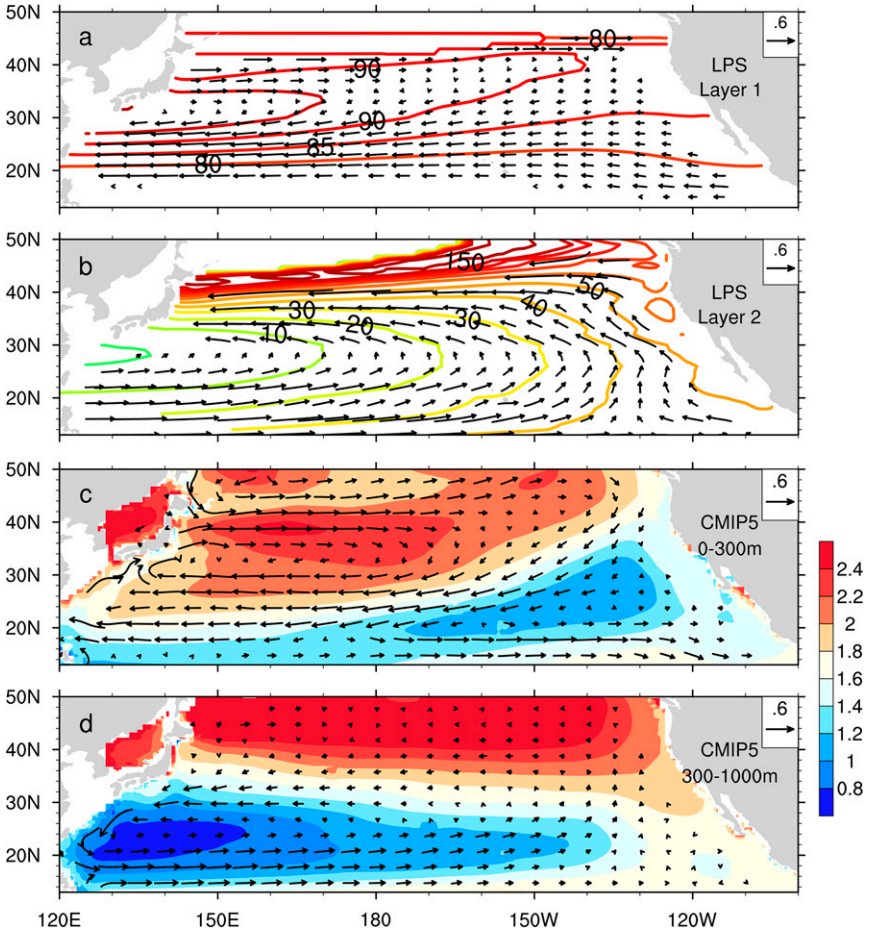

FIG. 8. (a),(b) Anomalous geostrophic streamlines (contours; m) and currents (vector; cm s^{-1}) from the ventilated model (LPS; Luyten et al. 1983) with full forcings. Anomalous circulation (vector; cm s^{-1}) and heat content (color; 10^9 J m^{-2}) in the (c) upper and (d) lower layers in CMIP5 ensemble mean. The anomaly is defined as the differences between the RCP4.5 and historical experiments.

further show that this forced response is insensitive to the spatial distribution of ocean surface warming, suggesting that the pattern of subsurface warming discussed here is likely robust.

A ventilated thermocline model suggests that both the strengthened stratification and downward heat mixing contribute to the pattern of the lower thermocline change. This simple model also predicts, and CMIP5 projections support, a baroclinic response to global warming with a spinup and spindown of the subtropical gyre in the upper and lower thermocline, respectively. This has important implications for climate change–observing systems. Satellite altimetry can detect the surface circulation change, but it requires sustained subsurface observations, such as Argo floats, to capture the lower thermocline spindown. It is important to develop effectively observation systems to monitor and detect ocean changes toward a deeper physical understanding and more reliable prediction of climate and environment changes.

Acknowledgments. We acknowledge the World Climate Research Programme Working Group on Coupled Modelling, which is responsible for CMIP. We thank Y. Kosaka for downloading CMIP datasets. The work was supported by the National Basic Research Program of China (2012CB955600), the National Natural Science Foundation of China (41125019, 41206021), and the U.S. National Science Foundation (AGS 1249145, 1305719). We thank Dr. David P. Marshall and the two anonymous reviewers for their constructive comments.

REFERENCES

Balmaseda, M. A., K. E. Trenberth, and E. Källén, 2013: Distinctive climate signals in reanalysis of global ocean heat content. *Geophys. Res. Lett.*, **40**, 1754–1759, doi:10.1002/grl.50382.

Barnier, B., and Coauthors, 2007: Eddy-permitting ocean circulation hindcasts of past decades. *CLIVAR Exchanges*, No. 42, International CLIVAR Project Office, Southampton, United Kingdom, 8–10.

Blanke, B., and P. Delecluse, 1993: Variability of the tropical Atlantic Ocean simulated by a general circulation model with two different mixed-layer physics. *J. Phys. Oceanogr.*, **23**, 1363–1388, doi:10.1175/1520-0485(1993)023<1363:VOTTAO>2.0.CO;2.

Church, J. A., J. S. Godfrey, D. R. Jackett, and T. J. McDougall, 1991: A model of sea level rise caused by ocean thermal expansion. *J. Climate*, **4**, 438–456, doi:10.1175/1520-0442(1991)004<0438:AMOSLR>2.0.CO;2.

——, and Coauthors, 2011: Revisiting the Earth's sea-level and energy budgets from 1961 to 2008. *Geophys. Res. Lett.*, **38**, L18601, doi:10.1029/2011GL048794.

Corno, G., D. M. Karl, M. J. Church, R. M. Letelier, R. Lukas, R. R. Bidigare, and M. R. Abbott, 2007: Impact of climate forcing on ecosystem processes in the North Pacific Subtropical Gyre. *J. Geophys. Res.*, **112**, C04021, doi:10.1029/2006JC003730.

Cowan, T., W. Cai, A. Purich, L. Rotstayn, and M. H. England, 2013: Forcing of anthropogenic aerosols on temperature trends of the sub-thermocline southern Indian Ocean. *Sci. Rep.*, **3**, 245, doi:10.1038/srep02245.

Crandall, B., J. Molinari, and D. Vollaro, 2014: Forecasting challenges associated with tropical cyclones within subtropical gyres. *Wea. Forecasting*, **29**, 99–114, doi:10.1175/WAF-D-13-00053.1.

Deser, C., A. S. Phillips, and M. A. Alexander, 2010: Twentieth century tropical sea surface temperature trends revisited. *Geophys. Res. Lett.*, **37**, L10701, doi:10.1029/2010GL043321.

Durack, P. J., S. E. Wijffels, and R. J. Matear, 2012: Ocean salinities reveal strong global water cycle intensification during 1950–2000. *Science*, **336**, 455–458, doi:10.1126/science.1212222.

Flato, G., and Coauthors, 2013: Evaluation of climate models. *Climate Change 2013: The Physical Science Basis*, T. F. Stocker et al., Eds., Cambridge University Press, 741–866.

Gent, P., and J. Mcwilliams, 1990: Isopycnal mixing in ocean circulation models. *J. Phys. Oceanogr.*, **20**, 150–155, doi:10.1175/1520-0485(1990)020<0150:IMIOCM>2.0.CO;2.

Gnanadesikan, A., 1999: A simple predictive model for the structure of the oceanic pycnocline. *Science*, **283**, 2077–2079, doi:10.1126/science.283.5410.2077.

Huang, R. X., 2010: *Ocean Circulation: Wind-Driven and Thermohaline Processes.* Cambridge University Press, 791 pp.

Karl, D. M., R. Letelier, D. Hebel, L. Tupas, J. Dore, J. Christian, and C. Winn, 1995: Ecosystem changes in the North Pacific subtropical gyre attributed to the 1991-92 El Niño. *Nature*, **373**, 230–234, doi:10.1038/373230a0.

Kobashi, F., and A. Kubokawa, 2012: Review on North Pacific subtropical countercurrents and subtropical fronts: Role of mode waters in ocean circulation and climate. *J. Oceanogr.*, **68**, 21–43, doi:10.1007/s10872-011-0083-7.

Large, W. G., and S. Yeager, 2009: The global climatology of an interannually varying air-sea flux data set. *Climate Dyn.*, **33**, 341–364, doi:10.1007/s00382-008-0441-3.

Letelier, R. M., D. M. Karl, M. R. Abbott, P. Flament, M. H. Freilich, R. Lukas, and P. T. Strub, 2000: Role of late winter mesoscale events in the biogeochemical variability of the upper water column of the North Pacific Subtropical Gyre. *J. Geophys. Res.*, **105**, 28 723–28 740, doi:10.1029/1999JC000306.

Levitus, S., and Coauthors, 2012: World ocean heat content and thermosteric sea level change (0–2000 m), 1955–2010. *Geophys. Res. Lett.*, **39**, L10603, doi:10.1029/2012GL051106.

Luo, Y., Q. Liu, and L. M. Rothstein, 2009: Simulated response of North Pacific Mode Waters to global warming. *Geophys. Res. Lett.*, **36**, L23609, doi:10.1029/2009GL040906.

Luyten, J. R., J. Pedlosky, and H. Stommel, 1983: The ventilated thermocline. *J. Phys. Oceanogr.*, **13**, 292–309, doi:10.1175/1520-0485(1983)013<0292:TVT>2.0.CO;2.

Madec, G., 2008: NEMO ocean engine. Version 3.0, Note du Pôle de Modélisation 27, Institut Pierre-Simon Laplace, 209 pp.

Marshall, D. P., and L. Zanna, 2014: A conceptual model of ocean heat uptake under climate change. *J. Climate*, **27**, 8444–8465, doi:10.1175/JCLI-D-13-00344.1.

Munk, W. H., 1966: Abyssal recipes. *Deep Sea Res.*, **13**, 707–730.

Qiu, B., and S. Chen, 2005: Variability of the Kuroshio Extension jet, recirculation gyre, and mesoscale eddies on decadal time scales. *J. Phys. Oceanogr.*, **35**, 2090–2103, doi:10.1175/JPO2807.1.

——, and ——, 2013: Concurrent decadal mesoscale eddy modulations in the western North Pacific subtropical gyre. *J. Phys. Oceanogr.*, **43**, 344–358, doi:10.1175/JPO-D-12-0133.1.

Sakamoto, T. T., H. Hasumi, M. Ishii, S. Emori, T. Suzuki, T. Nishimura, and A. Sumi, 2005: Responses of the Kuroshio and the Kuroshio Extension to global warming in a high-resolution climate model. *Geophys. Res. Lett.*, **32**, L14617, doi:10.1029/2005GL023384.

Sun, S., L. Wu, and B. Qiu, 2013: Response of the inertial recirculation to intensified stratification in a two-layer quasigeostrophic ocean circulation model. *J. Phys. Oceanogr.*, **43**, 1254–1269.

Taguchi, B., S.-P. Xie, N. Schneider, M. Nonaka, H. Sasaki, and Y. Sasai, 2007: Decadal variability of the Kuroshio Extension: Observations and an eddy-resolving model hindcast. *J. Climate*, **20**, 2357–2377, doi:10.1175/JCLI4142.1.

Taylor, K. E., R. J. Stouffer, and G. A. Meehl, 2012: An overview of CMIP5 and the experiment design. *Bull. Amer. Meteor. Soc.*, **93**, 485–498, doi:10.1175/BAMS-D-11-00094.1.

Terray, L., L. Corre, S. Cravatte, T. Delcroix, G. Reverdin, and A. Ribes, 2012: Near-surface salinity as nature's rain gauge to detect human influence on the tropical water cycle. *J. Climate*, **25**, 958–977, doi:10.1175/JCLI-D-10-05025.1.

Timmermann, A., and Coauthors, 2007: The influence of a weakening of the Atlantic meridional overturning circulation on ENSO. *J. Climate*, **20**, 4899–4919, doi:10.1175/JCLI4283.1.

——, S. McGregor, and F.-F. Jin, 2010: Wind effects on past and future regional sea level trends in the southern Indo-Pacific. *J. Climate*, **23**, 4429–4437, doi:10.1175/2010JCLI3519.1.

Tokinaga, H., S.-P. Xie, C. Deser, Y. Kosaka, and Y. M. Okumura, 2012: Slowdown of the Walker circulation driven by tropical Indo-Pacific warming. *Nature*, **491**, 439–443, doi:10.1038/nature11576.

Vallis, G. K., 2006: *Atmospheric and Oceanic Fluid Dynamics.* Cambridge University Press, 745 pp.

Xu, L. X., S.-P. Xie, and Q. Liu, 2012: Mode water ventilation and subtropical countercurrent over the North Pacific in CMIP5 simulations and future projections. *J. Geophys. Res.*, **117**, C12009, doi:10.1029/2012JC008377.

Yin, J. Y., S. M. Griffies, and R. J. Stouffer, 2010: Spatial variability of sea level rise in twenty-first century projections. *J. Climate*, **23**, 4585–4607, doi:10.1175/2010JCLI3533.1.

Zhang, R., and T. L. Delworth, 2005: Simulated tropical response to a substantial weakening of the Atlantic thermohaline circulation. *J. Climate*, **18**, 1853–1860, doi:10.1175/JCLI3460.1.

Zhang, X., J. A. Church, S. M. Plattern, and D. Monselesan, 2014: Projection of subtropical gyre circulation and associated sea level changes in the Pacific based on CMIP3 climate models. *Climate Dyn.*, **43**, 131–144, doi:10.1007/s00382-013-1902-x.